NANO LETTERS

pubs.acs.org/NanoLett

Symmetry Relationship and Strain-Induced Transitions between Insulating M1 and M2 and Metallic R phases of Vanadium Dioxide

A. Tselev,*,† I. A. Luk'yanchuk,†,§ I. N. Ivanov,† J. D. Budai,† J. Z. Tischler,† E. Strelcov,‖ A. Kolmakov,‖ and S. V. Kalinin†

†Oak Ridge National Laboratory, Oak Ridge, Tennessee 37831, United States, †Laboratory of Condensed Matter Physics, University of Picardie Jules Verne, Amiens, 80039, France, §L. D. Landau Institute for Theoretical Physics, Moscow, Russia, and ‖Physics Department, Southern Illinois University Carbondale, Carbondale, Illinois 62901, United States

ABSTRACT The ability to synthesize VO_2 in the form of single-crystalline nanobeams and nano- and microcrystals uncovered a number of previously unknown aspects of the metal−insulator transition (MIT) in this oxide. In particular, several reports demonstrated that the MIT can proceed through competition between two monoclinic (insulating) phases M1 and M2 and the tetragonal (metallic) R phase under influence of strain. The nature of such phase behavior has been not identified. Here we show that the competition between M1 and M2 phases is purely lattice-symmetry-driven. Within the framework of the Ginzburg−Landau formalism, both M phases correspond to different directions of the same four-component structural order parameter, and as a consequence, the M2 phase can appear under a small perturbation of the M1 structure such as doping or stress. We analyze the strain-controlled phase diagram of VO_2 in the vicinity of the R−M2−M1 triple point using the Ginzburg−Landau formalism and identify and experimentally verify the pathways for strain-control of the transition. These insights open the door toward more systematic approaches to synthesis of VO_2 nanostructures in desired phase states and to use of external fields in the control of the VO_2 phase states. Additionally, we report observation of the triclinic T phase at the heterophase domain boundaries in strained quasi-two-dimensional VO_2 nanoplatelets, and theoretically predict phases that have not been previously observed.

KEYWORDS Vanadium dioxide, metal-insulator phase transition, structural transformations, symmetry relationships, Landau-Ginzburg theory, stress-induced phase stabilization

Vanadium dioxide VO_2 is a prototypical strongly correlated electron oxide, which exhibits an abrupt, first-order metal−insulator transition (MIT) on cooling at a temperature of about $T_c = 68$ °C in bulk with a few orders of magnitude change of electrical conductivity within a sub-100-fs intrinsic time scale.[1,2] These features make this material an excellent candidate for numerous applications in optical, electronic, and optoelectronic devices. However, the drop in conductivity is accompanied by a symmetry-lowering—tetragonal-to-monoclinic—lattice structure transformation, and although, there is strong evidence that the main driving force for the transition is electron−electron correlations, the low-temperature phase should not be considered as a conventional Mott insulator due to a significant lattice contribution in the formation of the band gap. In fact, remaining an actively debated topic, the exact physical mechanism of the MIT is still not completely understood,[2−9] which hampers many of the potential applications of the material.

In particular, due to proximity of the MIT to room temperature and a fast rate of resistivity change through the MIT, VO_2 is considered the most promising candidate for realization of a Mott field-effect transistor, i.e., an electronic switch based on an electrostatically induced MIT.[10,11] It has been indeed demonstrated that MIT without a structural transformation can be induced by electrostatic or photonic doping,[2,5,10,12] but participation of lattice degrees of freedom in band gap formation turns out to be a significant obstacle in achieving a MIT without a change of the lattice structure based on the monoclinic phase M1, the phase that is stable in pure VO_2 under ambient temperature and pressure.[2,6]

A prominent feature in the structure of the M1 phase is chains of dimerized V atoms creating a twisted arrangement along the *c* axis of the parent tetragonal rutile structure (R).[13] In the other known monoclinic structure M2, only half of the V atoms are paired in strictly linear chains along the rutile *c* axis, whereas the other half makes a twisted arrangement similar to that present in M1, but with all nearest V−V distances being equal. While the pairing of vanadium atoms, as was initially suggested, may contribute the band gap formation in the M1 phase through a Peierls mechanism,[14] the M2 structure is a clear Mott insulator.[15] It was proposed that the investigation of the M2 phase may provide a clue to understanding of the R-to-M1 transition observed in the bulk.[15,16] Also due to being a Mott insulator, the M2 phase

* Corresponding author, tseleva@ornl.gov.
Received for review: 06/9/2010
Published on Web: 10/12/2010

DOI: 10.1021/nl1020443 | *Nano Lett.* **2010,** *10,* 4409–4416

is considered a more suitable than the M1 phase for the realization of a Mott transistor.[11]

Elastic strain plays a major role in controlling the phase transition in the VO_2 system. With use of techniques sensitive to local symmetry, it was shown first by Pouget et al.[17] in 1975 that a symmetry-breaking uniaxial stress applied in the $[110]_R$ direction leads to formation of the M2 phase structure in pure VO_2 with appearance of a transitional triclinic phase T. Recently developed methodology for growth of VO_2 single-crystalline nanobeams of a nanometer-scale size in the lateral cross section, which is below the characteristic hetero- and homophase domain sizes in the system,[18] allowed direct observation of strain-induced effects in the MIT. In particular, in the pioneering work by Wu et al.,[19] it was shown that in VO_2 nanobeams strongly attached to the substrate, the substrate−nanobeam mechanical interaction leads to formation of self-organized quasi-periodic domain structures of the metallic and insulating phases and strongly broadens the transition over temperature. Later, several previously unknown fundamental aspects of the MIT in the system were revealed in the end-clamped suspended nanobeams with use of lateral strains (strains in the $[001]_R$ direction) developing as a result of the phase transition.[8] Further, the M2 phase was observed competing with the M1 phase in the VO_2 nanobeams as a part of the heterophase domain structure,[11,20] and the authors ascribed the M2 phase appearance to the surface-stress effects[20] and to longitudinal stresses due to clamping of the nanobeams to the substrate.[11] The importance of the longitudinal strains in the phase sequence upon transition and in the appearance of the M2 phase was studied in more detail by Jones et al.[21] with use of substrate-attached microcrystals. Finally, Cao and co-workers[22] obtained a phase diagram of the M1, M2, R phases under uniaxial stress applied in the $[001]_R$ direction over an extremely wide range of stresses using the idea of strain engineering in bent nanobeams.[23] In several reports it was shown that the M2 phase can be stabilized down to room temperature.[11,21,24] Moreover, using VO_2 nanobeams, it was demonstrated that the M2 phase can be driven metallic by carrier injection without a structural a change.[11]

Despite the wealth of the experimental information, the nature of the M1/M2 phase competition has not been identified thus far, and the effective use of M1-R and M2-R phase transformation in VO_2 is limited by the lack of thermodynamic theory that rationalizes and predicts the role of external fields on phase transformation sequence.

We note that due to the structural transitions at the MIT, VO_2 is an improper ferroelastic. Theories based on the Ginzburg−Landau (GL) approach are very successful for ferroic transformations in general and in fact turned out to be essential both for applications and for basic science of ferroics materials.[25,26] They allow analysis of phase morphology, effect of external variables, type and structure of topological defects, as well as phase-field like modeling. A cornerstone of the GL approach is the material-specific change of the symmetry in the system at a phase transition with deviation from higher- to lower-symmetry phase quantitatively described by a parameter called *order parameter*, whose value is equal to zero in the higher-symmetry phase. Symmetry-determined mathematical properties of the order parameter provide vital information about the system behavior at the phase transition.[27] Dimensionality of the order parameter and the exact form of the free-energy polynomial, which in turn is determined by the symmetry of the lower-temperature phase, can be used to construct phase diagrams and make predictions about behavior of the particular system without going into exact quantitative treatment of the problem. New phases can be predicted as well. On the other hand, GL approach is complementary to microscopic theories and ab initio calculations. It allows one to work close to the transition temperature where the microscopic theory and ab initio calculations usually fail. (They are more effective at $T = 0$.) In addition, by simple means, it permits the construction of a theory for complex highly degenerate systems and correctly define the orthogonal basis functions that should be used thereafter in the microscopic theory.

In this Letter, we show that the relative stabilization of M1 and M2 phases in VO_2 can be interpreted in the framework of the GL phase transition theory as a result of renormalization of coefficients in the corresponding Landau free energy functional in response to external system perturbations. The symmetry analysis unambiguously indicates that M1 and M2 phases are two different ways to resolve the same instability of the rutile phase lattice. The critical temperatures of the phases are equal. The lower-symmetry phases participating in the transformation can be stabilized in respect to each other by perturbations. Further, to demonstrate control over the formation of M2 phase, we show that the M2 phase can be stabilized in the vicinity of the triple point in coexistence with M1 and R phases in tensile-strained single-crystalline quasi-two-dimensional VO_2 nanoplatelets (NPls). These novel insights into the relationship between M1, M2, and R phases of VO_2 can allow a straightforward interpretation of experimental observations on VO_2 poly- and single-crystalline samples, prediction of appearance of the phases in different experimental settings, and more systematic approaches to synthesis of VO_2 samples in desired phase states.

Ginzburg−Landau Theory Description of the Phase Transition. We start with first noting that the insulating phases M1 and M2 are very closely related by the internal lattice symmetry of their parent metallic phase of the rutile lattice structure. The transformation relation for lattice basis vectors for the parent and daughter phases are[13]

$$\begin{pmatrix}\mathbf{a}\\ \mathbf{b}\\ \mathbf{c}\end{pmatrix}_{M1} = \begin{pmatrix}0 & 0 & 2\\ 1 & 0 & 0\\ 0 & 1 & -1\end{pmatrix}\begin{pmatrix}\mathbf{a}\\ \mathbf{b}\\ \mathbf{c}\end{pmatrix}_{R}, \quad \begin{pmatrix}\mathbf{a}\\ \mathbf{b}\\ \mathbf{c}\end{pmatrix}_{M2} = \begin{pmatrix}2 & 0 & 0\\ 0 & 0 & 2\\ 0 & -1 & 0\end{pmatrix}\begin{pmatrix}\mathbf{a}\\ \mathbf{b}\\ \mathbf{c}\end{pmatrix}_{R} \tag{1}$$

DOI: 10.1021/nl1020443 | *Nano Lett.* **2010,** *10,* 4409–4416

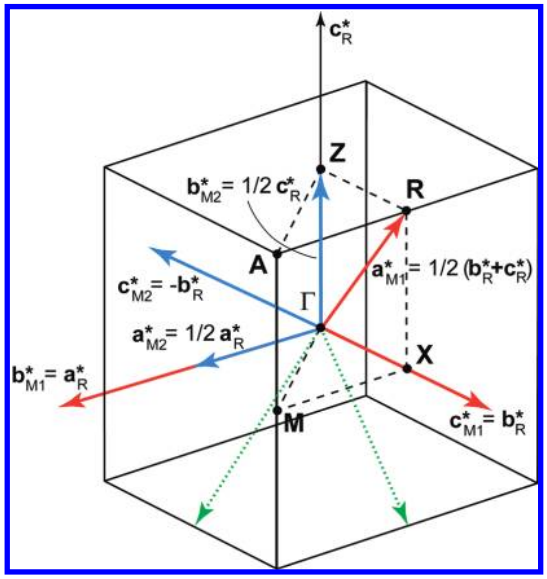

FIGURE 1. Relation between reciprocal lattices of M1, M2, and R structures. The diagram shows basis vectors of the reciprocal lattices related to the rutile Brillouin zone (lattice distortions due to strain are ignored). As is evident, vectors $\vec{a}_{M1}$* and $\vec{a}_{M2}$* + $\vec{b}_{M2}$* are compatible with the k-point *R* of the rutile Brillouin zone. The star of the *k*-vector at the point *R* is shown with dotted line arrows.

In unconstrained bulk VO_2 samples the first-order transition occurs from R into M1. In the framework of the GL theory, the displacive transformation from phase R with space group $P4_2/mnm$ (#136) to phase M1 with space group $P2_1/c$ (#14) is induced by a lattice instability at the special point $R(0,1/2,1/2)$ in the rutile tetragonal Brillouin zone (Figure 1).[28,29] Specifically, the distortion mode responsible for the change of the symmetry is associated with the irreducible representation (irrep) R_1^- of the group $P4_2/mnm$. Lattice distortions leading to the monoclinic phase M2 with symmetry group $C2/m$ (#12) correspond to the same special point R of the rutile Brillouin zone[30] as is evident from Figure 1. This result can be readily obtained from eq 1 by applying the Miller−Kwok theorem.[31] Further analysis of isotropy subgroups of the group $P4_2/mnm$,[29,32] shows that both of the phases are induced by the same irrep R_1^- of the group $P4_2/mnm$. It follows then that the structural transformations from the tetragonal to both monoclinic phases are driven by the same microscopic mechanism and stabilization of one of the monoclinic structures with respect to the other can be controlled by small perturbations such as doping or external stress as indeed is evidenced by the available experimental data. While M1 is the stable low-temperature phase in pure VO_2, M2 was previously stabilized by light doping with Cr[13] or Al[33,34] or by application of a modest, 0.1 GPa, uniaxial pressure along a $\langle 110\rangle_R$ direction[17] as was shown to exist at room temperature in defective VO_2 crystals.[35] This suggests that in pure unconstrained VO_2 under ambient pressure, the M2 phase can correspond to a local minimum or to a saddle point of the free energy and become an absolute minimum due to a perturbation. We illustrate it in the following.

The irrep R_1^- of the group $P4_2/mnm$ is four-dimensional and the corresponding structural order parameter (OP) characterizing structural distortion of the lower-symmetry phases with respect to the higher-symmetry phase has four components. Under generators of the group $P4_2/mnm$, the OP $\vec{\eta} = (\eta_1,\eta_2,\eta_3,\eta_4) = (1234)$transforms to: $(3\bar{4}\bar{1}2)$ under $(C_{2x}|^1/_2, {}^1/_2, {}^1/_2)$, to $(\bar{2}14\bar{3})$ under C_{2b}, to (4321) under $(C_{4z}^-|^1/_2, {}^1/_2, {}^1/_2)$, and is multiplied by -1 for any of these operations conjugated with $(E|0, 0, 1)$. Two more virtually possible phases with symmetries *Fmmm* and $I4_1/a$ (denoted here O and TG, respectively), which are also maximal subgroups of the rutile group, are associated with the same irrep.[29] However, these symmetries have not been observed experimentally.

Normalized spontaneous values of the OP for the four phases M1, M2, O, and TG are expressed respectively as $\vec{\eta}_{M1} = (1/2^{1/2})(\eta,0,\eta,0)$, $\vec{\eta}_{M2} = (1/2^{1/2})(\eta,0,0,0)$, $\vec{\eta}_O = (1/2^{1/2})(\eta,\eta,0,0)$, and $\vec{\eta}_{TG} = (1/2^{1/2})(\eta,0,0,\eta)$. The OP subspace with $\eta_{2,4} = 0$, which contains phases M1 and M2, (with $\eta_1 \neq \eta_3 \neq 0$) corresponds to a structure with triclinic symmetry $P\bar{1}$. This phase, T, can be considered as a distorted M1 phase and appears in the phase diagrams of doped VO_2 as well as VO_2 under pressure.[13,17] All these phases have the same critical temperature T_c in respect to the transition from the R phase, and stabilization of the phase M1 in unconstrained pure VO_2 below the transition temperature is provided by nonlinear terms of the corresponding GL expansion of the free energy over the four-component OP

$$F = \frac{1}{2}A(T - T_c)\sum \eta_i^2 + \frac{1}{4}\sum b_{ij}\eta_i^2\eta_j^2 + \frac{1}{6}\sum d_{ij}\eta_i^2\eta_j^4 \quad (2)$$

Here, we expanded the free energy up to the sixth order to account for the discontinuous nature of transition with i, $j = 1...4$, $b_{ij} = b_{ji}$, $b_{11} = b_{22} = b_{33} = b_{44}$, $b_{12} = b_{34}$, $b_{13} = b_{24}$, $b_{14} = b_{23}$. The same rules are applied for d_{ij}. A small perturbation can remove the degeneracy of T_c or renormalize the relative strength of coefficients b_{ij}, d_{ij} and favor stabilization of another phase among M2, O, TG, and T. Interestingly, the analysis of the OP structure for M1 and M2 phases directly suggests that the zone-edge structural distortions leading to the M1 phase can be viewed as a superposition of two lattice distortions leading to the M2 phase, as was pointed out by Rice et al.[15]

We further demonstrate that a substrate-induced elastic strain $u = u_{zz}$ (the axis z is directed along the NPl length) can stabilize phase M2. For this purpose, we incorporate the strain-OP coupling $\approx \kappa u\sum\eta_i^2$ and the elastic energy $\approx (1/2)Cu^2$ ($C = C_{zzzz}$) into eq 2 and compare energies of the phase M1 with $\vec{\eta}_{M1} = (1/2^{1/2})(\eta,0,\eta,0)$ and of the phase M2 with $\vec{\eta}_{M2} = (1/2^{1/2})(\eta,0,0,0)$, assuming that energies of the phases O and TG are higher and not competitive with those of M1 and M2. (This can be always done by appropriate choice of the coefficients b_{ij} and d_{ij}). The

DOI: 10.1021/nl1020443 | *Nano Lett.* **2010,** *10,* 4409–4416

corresponding energy functional for the OP subspace of each phase can be written as

$$F_\alpha = \frac{1}{2}t\eta^2 + \frac{1}{4}b_\alpha\eta^4 + \frac{1}{6}d_\alpha\eta^6 + \kappa u\eta^2 + \frac{1}{2}Cu^2 \quad (3)$$

Here α = M1, M2, $t = a(T - T_c)$, $b_{M1} = (1/2)(b_{11} + b_{13})$, $b_{M2} = b_{11}$. The same rules but with a factor 1/4 are applied for d_α. The order parameter amplitude η and strain u are treated as variational parameters.

Equation 3 can be used to analyze the structural transition in bulk undoped and unrestricted VO_2. Since no external stress is applied, one can exclude the elastic degrees of freedom by minimization of eq 3 over u. In the resulting effective functionals

$$\tilde{F}_\alpha = t\eta^2/2 + \tilde{b}_\alpha\eta^4 + d_\alpha\eta^6/6$$

the renormalized fourth order coefficients $\tilde{b}_\alpha = b_\alpha - 2\kappa^2/C$ should be negative for the first-order transition. According to experimental observations, the phase M2 does not appear in bulk VO_2 samples, and the transition proceeds directly from R to M1. This is the case if at a supercooling temperature t_-,[36] when the transition instability occurs, the free energy of the phase M1 $\tilde{F}_{M1} = \tilde{b}_{M1}{}^3/12d_{M1}{}^2$ (as obtained by minimization of $\tilde{F}_\alpha$ over η at $t = 0$) is lower than that for the phase M2: $\tilde{F}_{M2} = \tilde{b}_{M2}{}^3/12d_{M2}{}^2$. Comparison of $\tilde{F}_{M1}$ and $\tilde{F}_{M2}$ gives the condition for suppression of the phase M2 in bulk

$$\beta^3 > \delta^2 \quad (4)$$

where $\tilde{b}_\alpha < 0$, $\beta = \tilde{b}_{M1}/\tilde{b}_{M2}$, and $\delta = d_{M1}/d_{M2}$.

This theory can be straightforwardly applied for the description of the phase transformations in the nanoscale for VO_2. We turn to the case of thin VO_2 nanoplatelets clamped to a substrate with an initial strain u_0 in the R phase just above transition temperature. Just below transition, the strained NPl breaks into domains of the R phase with a strain u and domains of either M1 or M2 phase with a strain u_M with a fraction p of the NPl volume being occupied by the high-temperature phase R. The thermodynamics of such a system is described by a functional

$$\Phi = F_\alpha(\eta, u)p + \frac{1}{2}Cu_M{}^2(1 - p)$$

where the energy $F_\alpha(\eta,u)$ is given by eq 3, and η, u, u_M, and p are the variational parameters, for which the clamping constraint

$$pu + (1 - p)u_M = u_0$$

is imposed. In a system without competing lower-symmetry phases, such a biphase mixture can exist in a temperature interval $t'_{c2} > t > t'_{c1}$ as has been determined in ref 36, and the upper critical temperature t'_{c2} is equal to the thermodynamic critical temperature

$$t_{0\alpha} = 3\tilde{b}_\alpha{}^2/16d_\alpha$$

of the free-sample functional eq 3. For several competing lower-symmetry phases corresponding to minima of eq 3, the phase with the highest t'_{c2} will nucleate first. This yields the condition of stabilization of phase M2 on cooling through the MIT as $t'_{c2,M1} < t'_{c2,M2}$ or

$$\beta^2 < \delta \quad (5)$$

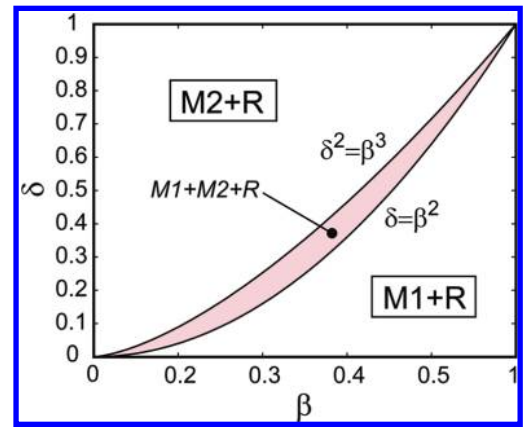

FIGURE 2. Phase diagram of strained VO_2 NPls in terms of theoretical parameters β and δ as defined in the text. In the shaded region, the coexistence of R, M1, and M2 domains is possible close to the MIT whereas the uniform phase M1 becomes stable at low temperatures. Below (above) this region only domains of M1 (M2) can coexist with domains of R close to the transition with further stabilization of the uniform phase M1 (M2) at low *T*.

The condition in eq 5 provides that in a strained NPl on cooling, the system from phase R goes first to a phase mixture R/M2, whereas because of condition eq 4 the uniform phase M1 is favored at low temperatures. At intermediate temperatures with $\beta, \delta < 1$, the conditions in eqs 4 and 5 can be valid simultaneously as illustrated in Figure 2, and M2 can coexist with M1 and R.

At the MIT, the rutile lattice instability leads to distortions associated with the zone-boundary R point in the primitive tetragonal Brillouin zone. These short-wavelength distortions reduce the point symmetry of the lattice, and long-wavelength distortions at the Brillouin zone center—spontaneous strains—will accompany zone-boundary distortions, if the latter are compatible with the lower point symmetry. Due to this coupling of zone-center and zone-boundary distortions, external restrictions such as stresses influence how exactly the transformation will occur at the zone-boundary and what be the resulting value of the order parameter. Therefore, not every strain configuration will be equivalently efficient in stabilization of one of the phases with respect to others.

Up to now we have accounted for the influence of an uniaxial longitudinal strain u_{zz} (or any strain like Au_{zz} +

DOI: 10.1021/nl1020443 | *Nano Lett.* **2010,** *10,* 4409–4416

$B(u_{xx}+u_{yy})$) that does not break the rutile tetragonal symmetry and therefore can only be considered as parameter that renormalizes the coefficients of the bare GL functional eq 2, but does not remove its symmetry. To elucidate the role of other symmetry breaking strains, we consider their conjugated coupling with the four-component order parameter invariant under the operations of $P4_2/mnm$:

$$F_{u\eta} = \frac{1}{2}\lambda_1(u_{xx}-u_{yy})(\eta_1^2-\eta_2^2+\eta_3^2-\eta_4^2) + \frac{1}{2}\lambda_2 u_{xy}(\eta_1^2+\eta_2^2-\eta_3^2-\eta_4^2) + \frac{1}{2}\lambda_3(u_{xz}\eta_1\eta_3-u_{yz}\eta_2\eta_4) \quad (6)$$

Integration of this energy into GL functional removes the degeneracy of critical temperature and stabilizes one of the phases M1, M2, or O (the phase with orthorhombic symmetry). Namely, stress u_{xz} always stabilizes one of the domains of phase M1. Stress $(u_{xx}-u_{yy})$ keeps the degeneracy of T_c for M1 and M2, but nonlinear terms b_{13}, d_{13} should stabilize phase M1 as in the unstrained sample. The most interesting case is presented by a shear stress u_{xy} that suppresses T_c for the M1 phase but keeps the degeneracy of T_c for the M2 and O phases. Stabilization of these phases depends on the coefficients b_{12}, d_{12}, but nevertheless, according to the symmetry considerations, application of u_{xy} should necessarily lead to intervention of either M2 or O phase below T_c. Experimentally, only the M2 phase has been observed. This is exactly the way pressure was applied by Pouget et al.,[17] when the M2 phase was originally obtained in pure VO_2 single crystals.

Note that for stabilization of the phase TG (with tetragonal symmetry, but with 4-fold-large R-phase unit cell), a conjugated symmetry-breaking field with the point symmetry group C_{4h} is required. Such a field cannot be produced by a uniform strain u_{ij} but can result from a nonuniformly distributed deformation, e.g., by a screw rotation of VO_2 nanobeams along the c_R axis.

Experiment. Proposed considerations explain well the sequence of transitions in the nanocrystalline forms of VO_2 reported in refs 11, 20, and 21. For further validation of the theory, we have performed additional studies of the temperature evolution of domain patterns in flat VO_2 nanocrystals (nanoplatelets, NPls) of a size larger than those in refs 11, 20, and 21. These crystals were grown on both rigid and flexible substrates in order to directly investigate the effect of strain on phase formation. To study and visualize the nucleation and dynamics of phase domains in the NPls, we used polarized light microscopy, micro-Raman spectroscopy, and X-ray microdiffraction.

Namely, VO_2 NPls were grown by vapor transport[18] using argon (13 Torr pressure, 3 sccm flux) as a carrier gas at a temperature of 1000 °C on Si/SiO_2 and quartz substrates as well as on more compliant 1 μm thick Si_3N_4 membranes supported by etched Si substrates. Raman spectra were collected using a confocal micro-Raman spectrometer (Renishaw 1000). The excitation was with a 632.8 nm HeNe laser focused in a ~1 μm diameter spot with a 100× objective. The laser power was kept at 7 μW to avoid local overheating. The laser polarization was parallel to the c_R axis with unpolarized detection. The X-ray microdiffraction measurements were carried out at the beamline 34-ID-E of the Argonne Advanced Photon Source using focused polychromatic synchrotron radiation.[37]

Most NPls remained firmly attached to the substrate after growth and cooling down to room temperature. X-ray microdiffraction indicated that the NPls are single-crystalline M1 phase at room temperature with the tetragonal c_R axis parallel to the long direction and the $\{110\}_R$ planes parallel to the substrate surface. The dimensions of NPls used in the experiments were typically a few micrometers wide, up to 100 μm long and about half micrometer thick. Detailed inspection of the NPls using polarized light optical microscopy and X-ray microdiffraction revealed that the NPls are typically twinned at room temperature with ferroelastic domain patterns compatible with the M1 phase, but not with the M2 phase.[36]

For rigid substrates used in the experiments, Si/SiO_2 and quartz, the difference in thermal expansion coefficients provides the in-plane anisotropic tensile stress in the NPls after cooling from growth temperature. Average linear expansion coefficients of Si and quartz in the temperature range from room temperature to 1000 °C are about 4×10^{-6} K^{-1} and 0.5×10^{-6} K^{-1}, respectively, which is significantly smaller than that of VO_2: 25×10^{-6} K^{-1} along the c_R direction and 4.5×10^{-6} K^{-1} along the a_R direction.[38] The tensile stress brings the system into the vicinity of the M1/M2/R triple point at temperatures close to T_c, where all three phases can be observed in coexistence.[17,21,22] Note that the expansion coefficient for quartz is about 1 order of magnitude smaller than that of VO_2 in the a_R direction; therefore, the NPls on this substrate experience in-plane, rather than uniaxial tensile strain.

The dimensions of our NPls are sufficiently large, so that the phases can be readily distinguished in a polarized light optical microscope as shown in Figure 3. The contrast between monoclinic and rutile phases arises due to their different optical density. Monoclinic phases cannot be resolved using unpolarized light. However due to their different birefringence, they can be distinguished in a polarized light microscope. For the particular crystallographic orientation of NPls in our experiment, M2 phase does not rotate polarization direction upon light reflection or transmission, whereas distinguishable variants of the orientational domains of the M1 phase do rotate it with opposite sense.[36] Phase identification was made using micro-Raman spectroscopy based on spectra of refs 39 and 40.

During the phase transition, the NPls are separated into heterophase domains along the NPl length similar to the

DOI: 10.1021/nl1020443 | Nano Lett. 2010, 10, 4409–4416

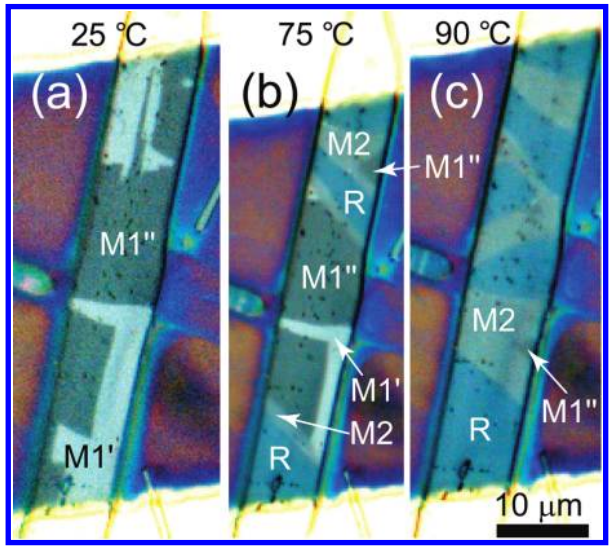

FIGURE 3. Polarized light images of a strained VO_2 NPl on a SiO_2/Si substrate taken at temperatures (a) 25 °C, (b) 75 °C, and (c) 90 °C. Domains marked M1′ and M1″ are the only domain types present at room temperature and were identified as twin domains of the M1 phase. They cannot be distinguished in natural light. The domains denoted M2 are domains of the M2 phase, and in turn, they cannot be distinguished from M1 domains in natural light. The domains denoted R are domains of metallic phase, and they are visible as such in natural light. M1, M2, and R phases were identified with micro-Raman spectroscopy.

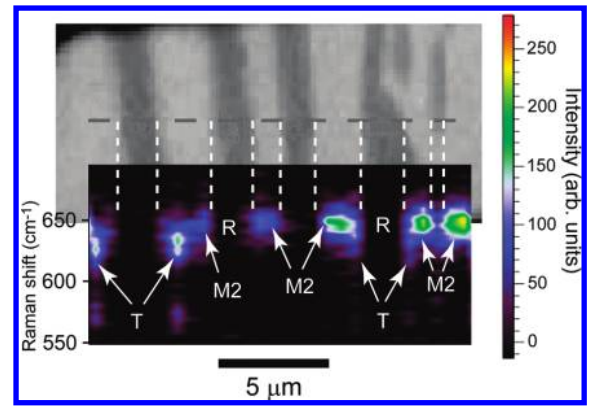

FIGURE 4. (upper panel) Unpolarized light image of metal and semiconductor domains in a VO_2 NPl grown on a quartz substrate. (lower panel) A 2D-map representation of Raman spectra taken along the line crossing metallic and insulating domains as indicated in the upper panel. The spectra were obtained in the interval where the M1 and M2 phases can be identified by distinct peaks at 615 and 649 cm^{-1}, respectively. The spectra of the R phase were corrected by normalization to the background. T is the distorted M1 phase. Substrate temperature is 72 °C.

nanobeams.[19] Generally, four types of domains are visible under polarized light in this case at an intermediate stage of the MIT as displayed in Figure 3b for an NPl on a Si/SiO_2 substrate. The usual scenario of the phase transition on heating begins with appearance of metallic R domains in the matrix of the M1 phase. The M2 phase appears at the boundaries between M1 and R domains, and then R and M2 domains grow by jump-wise motion of domain walls with the M2 phase consuming M1 as well as by nucleation of new metallic domains. At an advanced stage of the transition, the M1 phase is completely replaced by M2 phase in between metallic domains, and further growth of metallic domains takes place at the cost of the M2 phase. The phase sequence is reversed on cooling.

Despite the relatively large dimensions of the NPls, the phase sequences we observe are very similar to those observed in nanobeams with much smaller cross sections. It proves that size effects are not among major factors of the M2 phase formation in nanobeams and the phase sequence is controlled by strain.

Micro-Raman maps taken with ~0.5 μm spatial resolution frequently indicate the presence of the distorted M1 phase (T) at the boundaries between R and M2 domains as illustrated in Figure 4.

Preferential nucleation of the M2 phase at the M1/R boundaries can be readily explained by the relation between the lattice constants of the three phases along the c_R direction in the vicinity of the transition temperature: at $T \approx 70$ °C, $2c_R < a_{M1} < b_{M2}$ (5.70 Å < 5.75 Å < 5.80 Å).[13,38] M2 domains compensate for additional tensile stress due to the reduced lattice constant of the R phase in comparison with M1. (This interpretation is in accord with the discussion in ref 21.) However, this is not the only spot where the M2 phase could appear. Nucleation of the M2 phase directly in the M1 phase on heating with formation of large isolated domains of the M2 phase was also observed for NPls grown on quartz substrates, where the in-plane tensile stress in the direction perpendicular to the c_R axis is stronger than that for Si/SiO_2 substrates. Such stress is equivalent in its action to the u_{xy} shear stress, which suppresses the M1 phase as discussed above. Generally, details of the heterophase domain behavior can be very rich even among NPls of one sample, which indicates the influence of multiple factors such as local strain and strain distribution, chemical composition, and perfection of the lattice structure.

Figure 5 displays sequences of Raman spectra versus temperature taken at a fixed point on a VO_2 NPl grown on a quartz substrate. Note a very sharp transition within 0.1 °C (resolution of our thermal stage) between the M2 and R phases on heating in Figure 5a. The intensity of the M2 phase peaks does not change by approach to the transition temperature. This behavior indicates that the first-order transition takes place in a relatively large volume at once accompanied by a jump of a domain wall, without formation of small islands of the metallic phase in the insulating matrix as opposed to behavior observed in (inhomogeneous) polycrystalline thin films in ref 7.

As is evident from Figure 5b, the transition from the M2 phase on cooling occurs through a first-order jump into the distorted M1 phase T. The distortion gradually disappears until the M1 phase spectrum is formed without any noticeable change on further cooling. The latter transformation corresponds to the rotation of the order parameter vector in the four-dimensional subspace of the T phase in response

DOI: 10.1021/nl1020443 | *Nano Lett.* **2010,** *10,* 4409–4416

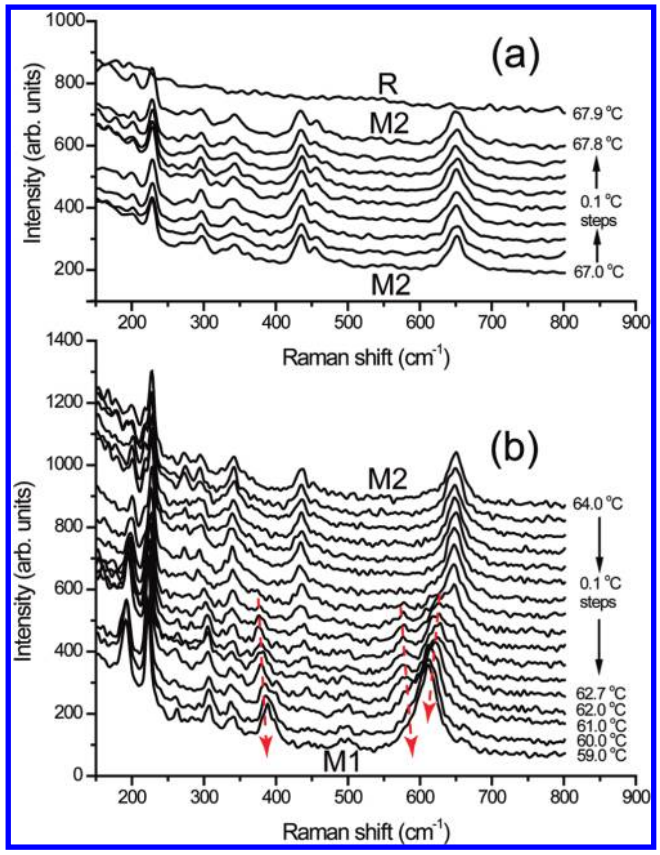

FIGURE 5. Sequences of Raman spectra vs temperature taken at a fixed point on a VO_2 NPl grown on a quartz substrate. The spectra illustrate the character of the phase transitions M2 ↔ R and M1 ↔ M2. (a) Transition M2 → R on heating is abrupt within 0.1 °C. (b) Transition M2 → M1 on cooling proceeds through formation of the distorted M1 phase (T), as is evidenced by first jump-like and then gradual shift and broadening of the V−O vibration mode peak at 610 cm^{-1}/650 cm^{-1}. Arrows also highlight appearance and gradual shift of two other prominent peaks of the M1 phase.

to the changing anisotropic stress until the two nonzero components of the order parameter become equal, which corresponds to the M1 phase. (Detailed theoretical investigation of the stress configuration leading to the formation of the T phase is now in progress.)

Next, we have performed X-ray microdiffraction structural measurements of individual heterophase domains on NPls grown on flexible Si_3N_4 membranes supported by etched 200 μm thick Si substrates. The scanning Laue diffraction patterns were taken with ~0.4 μm spatial resolution. These experiments confirmed the appearance of the M2 phase domains between R phase domains in the coexistence regime in NPls grown over the thick Si region of the substrates, where NPls are under a tensile stress. In contrast, the NPls on the flexible Si_3N_4 membrane parts of the same substrate were separated into metal and insulating domains during the phase transition; however, coexistence of only M1 and R phases was found in this case, which can be ascribed to insufficient external strain applied to in the NPls due the ability of the flexible membranes to bend and to partially release the strain in NPls. Thus, the observation of different sequences of monoclinic phase domains for crystals subjected to different substrate-induced strains in the same sample directly demonstrates how strain can control phase stabilization.

Additionally, the X-ray microdiffraction structural measurements revealed fine-scale twinning in the M2 domains with twin obliquity ~1.87° corresponding to the twin laws $[100]_{180°}$ or $[001]_{180°}$ (twin walls corresponding to $\{100\}_R$ crystallographic planes).[41] Previously, twinning of the M2 phase in nanobeams with the same twinning law was reported earlier in ref 22, and topographic indications of the twinning in the M2 phase domains were also found in VO_2 microcrystals in ref 21. Twining is an additional mechanism of strain accommodation during the phase transition, and it is generally expected to occur in the symmetry lowering structural transitions.[25] On the basis of diffraction peak intensities, in our NPls, the relative fractions of different orientational variants in the M2 phase domain volume were found to be unequal with ratios, which can be as low as 1:10, in contrast to bent nanobeams,[22] where the orientational variants of the phase M2 were found in the equal ratio.

In conclusion, within the framework of the Ginzburg−Landau phase transition theory, monoclinic phases M1 and M2 of VO_2 being lattice-symmetry-related correspond to the same multicomponent structural order parameter of the parent, R, phase, which indicates that the M1 and M2 phases are two different ways to resolve the same instability of the rutile phase lattice. Consequently, while in unconstrained VO_2, M1 is the stable lower-symmetry phase in ambient, a small perturbation renormalizes coefficients of the GL free energy functional and can stabilize the M2 phase with respect to the M1 phase or bring the M1, M2, and R phases into coexistence. A direct and important consequence of this fact is that any detailed interpretation of particular experimental data should account for contributions of all possible perturbations in the observed phase sequences. Taking into account that transformations R-M1 and R-M2 can be continuous even when these transitions are of the first order, another important consequence of this is that the phase M1 does not play any special role, such as an intermediate phase, in the MIT in comparison with the phase M1. This description is confirmed by the previously obtained experimental data as well as by our own experiments on strained VO_2 nanoplatelets.

Acknowledgment. Research at ORNL's Center for Nanophase Materials Sciences was sponsored by the Division of Scientific User Facilities, Office of Basic Energy Sciences, U.S. DOE. The work of I.L. was supported by ANR project LOMACOQU. The research at SIUC was supported through NSF ECCS-0925837 and SISGR-DOE ERKCM67. J.D.B. and J.Z.T. were supported by the Division of Materials Sciences and Engineering, Office of Basic Energy Sciences, U.S. DOE. Use of the APS beamline 34-ID-E was supported by the Scientific User Facilities Division of BES, U.S. DOE.

DOI: 10.1021/nl1020443 | *Nano Lett.* **2010,** *10,* 4409–4416

Supporting Information Available. Typical micro-Raman spectra of the M1, M2, and R phases, additional Raman spectra map, and Laue X-ray microdiffraction results. This material is free of charge via the Internet at http://pubs.acs.org.

REFERENCES AND NOTES

(1) Morin, F. J. *Phys. Rev. Lett.* **1959**, *3*, 34.
(2) Cavalleri, A.; Dekorsy, T.; Chong, H. H. W.; Kieffer, J. C.; Schoenlein, R. W. *Phys. Rev. B* **2004**, *70*, 161102.
(3) Zylbersztejn, A.; Mott, N. F. *Phys. Rev. B* **1975**, *11*, 4383.
(4) Biermann, S.; Poteryaev, A.; Lichtenstein, A. I.; Georges, A. *Phys. Rev. Lett.* **2005**, *94*, No. 026404.
(5) Kim, H.-T.; Lee, Y. W.; Kim, B.-J.; Chae, B.-G.; Yun, S. J.; Kang, K.-Y.; Han, K.-J.; Yee, K.-J.; Lim, Y.-S. *Phys. Rev. Lett.* **2006**, *97*, 266401.
(6) Kübler, C.; Ehrke, H.; Huber, R.; Lopez, R.; Halabica, A.; Haglund, R. F.; Leitenstorfer, A. *Phys. Rev. Lett.* **2007**, *99*, 116401.
(7) Qazilbash, M. M.; Brehm, M.; Chae, B.-G.; Ho, P. C.; Andreev, G. O.; Kim, B.-J.; Yun, S. J.; Balatsky, A. V.; Maple, M. B.; Keilmann, F.; Kim, H.-T.; Basov, D. N. *Science* **2007**, *318*, 1750.
(8) Wei, J.; Wang, Z.; Chen, W.; Cobden, D. H. *Nat. Nanotechnol.* **2009**, *4*, 420.
(9) Lazarovits, B.; Kim, K.; Haule, K.; Kotliar, G. *Phys. Rev. B* **2010**, *81*, 115117.
(10) Kim, H.-T.; Chae, B.-G.; Youn, D.-H.; Maeng, S.-L.; Kim, G.; Kang, K.-Y.; Lim, Y.-S. *New J. Phys.* **2004**, *6*, 52.
(11) Zhang, S.; Chou, J. Y.; Lauhon, L. J. *Nano Lett.* **2009**, *9*, 4527.
(12) Ruzmetov, D.; Gopalakrishnan, G.; Deng, J.; Narayanamurti, V.; Ramanathan, S. *J. Appl. Phys.* **2009**, *106*, No. 083702.
(13) Marezio, M.; McWhan, D. B.; Remeika, J. P.; Dernier, P. D. *Phys. Rev. B* **1972**, *5*, 2541.
(14) Goodenough, J. B. *J. Solid State Chem.* **1971**, *3*, 490.
(15) Rice, T. M.; Launois, H.; Pouget, J. P. *Phys. Rev. Lett.* **1994**, *73*, 3042.
(16) Eyert, V. *Ann. Phys.* **2002**, *11*, 650.
(17) Pouget, J. P.; Launois, H.; D'Haenens, J. P.; Merenda, P.; Rice, T. M. *Phys. Rev. Lett.* **1975**, *35*, 873.
(18) Guiton, B. S.; Gu, Q.; Prieto, A. L.; Gudiksen, M. S.; Park, H. *J. Am. Chem. Soc.* **2005**, *127*, 498.
(19) Wu, J.; Gu, Q.; Guiton, B. S.; de Leon, N. P.; Ouyang, L.; Park, H. *Nano Lett.* **2006**, *6*, 2313.
(20) Sohn, J. I.; Joo, H. J.; Ahn, D.; Lee, H. H.; Porter, A. E.; Kim, K.; Kang, D. J.; Welland, M. E. *Nano Lett.* **2009**, *9*, 3392.
(21) Jones, A. C.; Berweger, S.; Wei, J.; Cobden, D.; Raschke, M. B. *Nano Lett.* **2010**, *10*, 1574.
(22) Cao, J.; Gu, Y.; Fan, W.; Chen, L. Q.; Ogletree, D. F.; Chen, K.; Tamura, N.; Kunz, M.; Barrett, C.; Seidel, J.; Wu, J. *Nano Lett.* **2010**, *10*, 2667.
(23) Cao, J.; Ertekin, E.; Srinivasan, V.; Fan, W.; Huang, S.; Zheng, H.; Yim, J. W. L.; Khanal, D. R.; Ogletree, D. F.; Grossman, J. C.; Wu, J. *Nat. Nanotechnol.* **2009**, *4*, 732.
(24) Okimura, K.; Sakai, J.; Ramanathan, S. *J. Appl. Phys.* **2010**, *107*, No. 063503.
(25) Wadhawan, V. K. *Introduction to ferroic materials*; Gordon & Breach: Amsterdam, 2000.
(26) Tagantsev, A. K.; Fousek, J.; Cross, L. E. *Domains in Ferroic Crystals and Thin Films*; Springer: New York, 2010.
(27) Anderson, P. W. *Basic Notions of Condensed Matter Physics*, 2nd ed.; Westview Press: Boulder, CO, 1997.
(28) Brews, J. R. *Phys. Rev. B* **1970**, *1*, 2557.
(29) Stokes, H. T.; Hatch, D. M. *Isotropy subgroups of the 230 crystallographic space groups*; World Scientific Publishing Company: Singapore and Teaneck, NJ, 1988.
(30) McWhan, D. B.; Marezio, M.; Remeika, J. P.; Dernier, P. D. *Phys. Rev. B* **1974**, *10*, 490.
(31) Kwok, P. C.; Miller, P. B. *Phys. Rev.* **1966**, *151*, 387.
(32) Paquet, D.; Leroux-Hugon, P. *Phys. Rev. B* **1980**, *22*, 5284.
(33) Drillon, M.; Villeneuve, G. *Mater. Res. Bull.* **1974**, *9*, 1199.
(34) Ghedira, M.; Vincent, H.; Marezio, M.; Launay, J. C. *J. Solid State Chem.* **1977**, *22*, 423.
(35) Chamberland, B. L. *J. Solid State Chem.* **1973**, *7*, 377.
(36) Tselev, A.; Strelcov, E.; Luk'yanchuk, I. A.; Budai, J. D.; Tischler, J. Z.; Ivanov, I. N.; Jones, K.; Proksch, R.; Kalinin, S. V.; Kolmakov, A. *Nano Lett.* **2010**, *10*, 2003.
(37) Budai, J. D.; Liu, W.; Tischler, J. Z.; Pan, Z. W.; Norton, D. P.; Larson, B. C.; Yang, W.; Ice, G. E. *Thin Solid Films* **2008**, *516*, 8013.
(38) Kucharczyk, D.; Niklewski, T. *J. Appl. Crystallogr.* **1979**, *12*, 370.
(39) Schilbe, P. *Phys. B (Amsterdam, Neth.)* **2002**, *316-317*, 600.
(40) Marini, C.; Arcangeletti, E.; Di Castro, D.; Baldassare, L.; Perucchi, A.; Lupi, S.; Malavasi, L.; Boeri, L.; Pomjakushina, E.; Conder, K.; Postorino, P. *Phys. Rev. B* **2008**, *77*, 235111.
(41) Marezio, M.; Dernier, P. D. *Acta Crystallogr., Sect. A: Cryst. Phys., Diffr., Theor. Gen. Crystallogr.* **1973**, *29*, 618.

DOI: 10.1021/nl1020443 | *Nano Lett.* **2010,** *10,* 4409–4416